

1
2
3
4
5
6
7
8
9
10
11
12
13
14
15
16
17
18
19

**Observation and attribution of temperature trends near the stratopause from
HALOE**

by

Ellis Remsberg

Science Directorate, NASA Langley Research Center

21 Langley Blvd.

Hampton, Virginia 23681, USA

(corresponding author e-mail: ellis.e.remsberg@nasa.gov)

Key Points:

- HALOE temperature profiles span the stratopause region and indicate a near-global cooling of the order of -0.5 K/decade for 1993-2005.
- Trends for HALOE temperature and CH₄ are significant only in the southern hemisphere.
- The southern hemisphere T(p) trend agrees with that of the combined radiative forcings from CO₂, H₂O, and ozone.

20 **Abstract.** This study considers time series of temperature versus pressure, $T(p)$, from the
21 Halogen Occultation Experiment (HALOE) across the stratopause region, where the effects of
22 radiative forcings from the greenhouse gases (CO_2 and H_2O) and from ozone are most
23 pronounced. Trend analyses are from 1993-2005 for HALOE $T(p)$ values at seven levels from
24 3.0 to 0.3 hPa with a vertical resolution of about 4 km and for eight latitude zones from 65°S to
25 65°N . The HALOE trends at 2.0 hPa are of the order of -1.0 K/decade across the tropics and
26 subtropics, but then become smaller (-0.5 K/decade) at the middle latitudes. The near-global
27 HALOE trend profile has a minimum cooling rate of -0.2 K/decade at 1.0 hPa, although it is
28 more negative in the southern hemisphere and slightly positive in the northern hemisphere. The
29 combined radiative forcings from CO_2 , H_2O , and ozone are from -0.4 to -0.6 K/decade for 1993-
30 2005 and are hemispherically symmetric. HALOE temperature trend and total radiative cooling
31 profiles differ from those reported from observations and calculations for 1980-2000, mainly
32 because the ozone trends changed from clearly negative in the 1980s through mid-1990s to
33 slightly positive during the time of HALOE. Trends for the tracer, HALOE methane (CH_4),
34 increase from 2 to 4 %/decade from 50 hPa to 10 hPa, indicating an acceleration of the
35 Brewer/Dobson circulation. Analyses of time series of CH_4 across the stratopause reveal more
36 variability in the northern hemisphere, where wave dissipation likely contributes to the heating.

37 **1. Introduction**

38 A focus for chemistry climate model studies is how quickly is stratospheric ozone recovering and
39 what is the effect on temperature trends (e.g., Garcia et al., 2007; Langematz et al., 2003;
40 Maycock et al., 2018; Ramaswamy et al., 2001; Stolarski et al., 2010). Shine et al. (2003)
41 reported on model-simulated temperature trends in the stratopause region for 1980-2000, due to
42 the changes in ozone and in the greenhouse gases (GHG) or mainly in CO₂. Figure 1 shows the
43 total, area-weighted model temperature trend profile plus the separate contributions from ozone,
44 GHG, and H₂O, as adopted from Shine et al. (2003, their Figure 5). Trends in ozone mixing
45 ratio at 3 hPa and at 1 hPa are negative by about 7 to 4 %/decade, respectively, due to increases
46 in ozone depleting substances (ODS) during that period (Randel & Wu, 1999). Those decreases
47 in ozone add to the cooling trend rather than heating the stratopause region. Figure 1 also shows
48 a cooling contribution of about -0.2 K/decade from H₂O that had been increasing at the rate of ~1
49 %/year (Rosenlof et al., 2001).

50

51 Observed stratospheric temperature trends agree reasonably with the model-simulated total trend
52 profile in Figure 1 (e.g., see Seidel et al., 2016, their Figure 16). The observations are from
53 merged series of operational satellite radiance data and retrieved temperatures from stratospheric
54 sounding unit (SSU) and microwave sounding unit (MSU) sensors (e.g., Randel et al., 2009; Zou
55 & Qian, 2016). Seidel et al. (2016) found significant temperature trends of -0.7 to -1.2 K/decade
56 from 40°S to 40°N, respectively, from SSU channel 3 radiances (or SSU3 centered at 43 km in
57 altitude) for 1979-1994. Synthetic combinations of zonal-averaged radiances from several SSU
58 channels extended the temperature record across the stratopause (Nash & Saunders, 2015).

59

60 The Advanced Microwave Sounding Unit-A (AMSU-A) sensor began measurements in 1998,
61 although the top channel of AMSU-A (or channel 14 centered at 42 km) was not operational
62 until 2001. Since channel 14 does not extend as high as that of SSU3, Zou & Qian (2016)
63 matched the SSU and AMSU measurements in terms of temperature according to the vertical
64 weighting functions for their radiances and obtained a reliable long-term climate data record
65 (CDR). Their analogous SSU3-like temperature trends are smaller for the longer time span of
66 1979-2015 or about -0.7 K/decade ($2\sigma = \pm 0.08$) across the same latitude range (see Figure 9 of
67 Zou & Qian, 2016). Seidel et al. (2016) reported that the trends from MSU for 1995-2013 and
68 the trends from the merged SSU/AMSU record for 1995-2005 were smaller and not significant,
69 as the ODS and their effects on ozone were decreasing.

70

71 Randel et al. (2016) analyzed merged temperature time series from SSU/AMSU and compared
72 them with Microwave Limb Sounder (MLS) for 2004 and onward and with the Sounding of the
73 Atmosphere using Broadband Emission Radiometry (SABER) satellite observations for 2002
74 and onward. They integrated the higher vertical resolution profiles of MLS and SABER, so that
75 they were approximately consistent with the lower resolution, weighting functions of SSU and
76 AMSU-A. Then they applied a regression model to the merged time series from their equivalent
77 SSU3 channel and found global linear trends that decreased by -0.89 K/decade for 1979-1997,
78 but then slowed to -0.28 K/decade for 1998-2015. They also interpreted their trend changes to
79 the significant loss of upper stratospheric ozone in the earlier period as compared to slightly
80 increasing ozone values in the latter period. McLandress et al. (2015) merged SSU and AMSU

81 data records and reported that their temperature trends agreed with those from MLS for 2004-
82 2012. Yet, the present-day, merged CDRs do not extend to and above the stratopause for
83 completely resolving the changing effects from the primary forcing agents of the GHG, the ODS,
84 solar uv-flux, and planetary-scale wave forcings and are not optimal for detailed comparisons
85 with model results (e.g., Checa-Garcia et al., 2018; Aquila et al., 2016).

86

87 **2. Objectives**

88 This study focuses on analyses of temperature time series for the uppermost stratosphere and
89 lowermost mesosphere, as obtained with the single, Halogen Occultation Experiment (HALOE)
90 satellite instrument that operated from late 1991 through November 2005 (Russell et al., 1993) or
91 at a time when the effects of ODS on ozone were leveling off. HALOE temperature versus
92 pressure or T(p) profiles are from its version 19 (v19) algorithm, as described in Thompson &
93 Gordley (2009) and as validated in Remsberg et al. (2002). HALOE retrieved T(p) is from
94 transmission measurements versus scan angle (or altitude) from its 2.8- μm CO₂ channel.
95 However, since there are slight inaccuracies for the HALOE forward model of CO₂ transmission
96 in the middle stratosphere, there is a merger of the HALOE-retrieved temperatures with the
97 NOAA Climate Prediction Center (CPC) temperature profiles supplied to the HALOE Project
98 during the mission life of its Upper Atmosphere Research Satellite (UARS). Remsberg &
99 Deaver (2005) reported one instance of a discontinuity in the HALOE T(p) time series near May
100 2001. Figure 2 is an update of their data series at the 5-hPa level and centered at 22.5°N; the
101 oscillatory curve is a fit to those data. The straight-line fit is just the constant plus trend term,
102 and the trend is unrealistically large (-3.7 K/decade). However, the final, merged HALOE/CPC

103 T(p) profiles are entirely based on transmission measurements from the HALOE CO₂ channel
104 beginning at about 2 hPa (~43 km) (Thompson & Gordley, 2009). They extend upward through
105 the entire mesosphere, and their time series show no discontinuities. The forward model for the
106 HALOE T(p) algorithm also accounts for annual changes of atmospheric CO₂ with a 4-yr lag to
107 account for its slow net ascent from the troposphere to the middle stratosphere. In addition,
108 Gordley et al. (2009) reported that there are no detectable false trends due to instrumental effects
109 for the HALOE radiometer channels for CO₂, ozone, and H₂O.

110

111 HALOE T(p) has a vertical resolution of about 4 km or comparable with the profiles from MLS
112 and SABER. The HALOE temperature time series bracket the time of transition from SSU to
113 AMSU-A, and when ODS were leveling off and starting to decline. Proper comparisons of T(p)
114 from SSU and AMSU-A with the HALOE results require that the HALOE profiles be convolved
115 with the lower vertical resolution weighting functions of those operational temperature sounders.
116 But, the weighting functions for SSU3 and AMSU (channel 14) extend well below the 3-hPa
117 level, such that only qualitative comparisons are achievable. The present study focuses only on
118 the trends of T(p) from HALOE in the uppermost stratosphere and lower mesosphere.

119

120 Remsberg (2008a, Figure 16) analyzed HALOE temperatures from 1991-2005 and found
121 significant cooling trends at 1 to 2 hPa of the order of -0.5 to -1.0 K/decade. For that early study,
122 he simply fit a periodic 11-yr term to the data, rather than considering a proxy solar cycle term,
123 and he noted that his 11-yr term for the middle latitudes was not exactly in-phase with the solar
124 flux proxy—perhaps due to dynamical effects. Another concern with his initial study is that the

125 11-yr and linear trend terms are collinear and alias to each other. The updated analyses herein
126 make use of time series of the Lyman- α flux as the proxy term for the 11-yr solar cycle forcing
127 plus a multivariate ENSO index (or MEI) term for the multiple linear regression (MLR)
128 modeling. There are also perturbations from the June 1991 eruption of Mt. Pinatubo that affect
129 the temperature time series of both HALOE and SSU3/AMSU (e.g., Lee & Smith, 2003; Zou &
130 Qian, 2016). Those atmospheric effects extend several years in the operational temperature
131 record because the SSU3 measurements have contributions that extend into the middle
132 stratosphere. For this reason, Randel et al. (2016) excluded two years of data following the 1991
133 eruption for their analyses of SSU3. Volcanic influences are not apparent in HALOE T(p) time
134 series near the stratopause after 1992.

135
136 Section 3 describes briefly the present regression modeling of HALOE T(p) from January 1993
137 to November 2005 and does not include a proxy volcanic term. Although the HALOE algorithm
138 provides temperature profiles for the upper stratosphere and mesosphere that are well sampled
139 and in hydrostatic balance, the MLR trend analyses herein are limited to seven, discrete pressure
140 altitudes from 3.0 to 0.3 hPa and across eight different latitude zones to give a set of 56 separate
141 time series. In addition to the analyzed trends, Section 3 reports on the responses of temperature
142 to variations of the solar flux and compares them with results from SABER. Section 4 shows
143 analyzed HALOE temperature trends across the stratopause and as a function of latitude.

144 Merged SSU3/AMSU data for the time span of HALOE are also fit using the same regression
145 model for purposes of their qualitative comparison; absolute temperatures from SSU3/AMSU are
146 comparable to HALOE values from just below the 3-hPa level (near 40 km). As expected, the
147 near-global T(p) trends from HALOE are not as negative as the model-simulated trends for

148 1980-2000 of Shine et al. (2003) because the changes in ozone were slowing to near zero in the
149 upper stratosphere. Section 5 reports on the associated trends for ozone and water vapor from
150 the HALOE data. Near-global estimates of their radiative effects are added to those of CO₂ from
151 Shine et al. (2003) to give an estimate of total forcing for comparison with the observed
152 hemispheric and global HALOE T(p) trend profiles. Section 6 considers HALOE methane
153 (CH₄) as a tracer for evaluating whether dynamical activity might be affecting the T(p) trends.
154 Section 7 summarizes the findings about the trends in T(p) and their attribution across the
155 stratopause from the HALOE data.

156

157 **3. Analysis approach**

158 HALOE v19 T(p) profiles are grouped into six, separate 15°-wide latitude bins (centered from
159 37.5°S to 37.5°N) plus two 20°-wide bins centered at 55° latitude to obtain time series of zonal-
160 average estimates of T(p) and at seven levels from 3.0 to 0.3 hPa. The wider bins at 55° provide
161 for adequate seasonal sampling in the latter years of the HALOE mission. As in Remsberg
162 (2008a), the separate sunset (SS) and sunrise (SR) points in a time series are according to the
163 dates when the tangent layer of those HALOE occultation events occur in a given latitude zone.
164 Each data point within the zone is a “bin-average” of at least five profiles (usually many more).
165 The separate SS and SR time series undergo an initial MLR fitting. Then there is an adjustment
166 of the SS and SR data points by one-half the difference of the means of their separate series. To
167 first order, this approach accounts for the “short-period noise” of the diurnal effects from a series
168 of alternating, SS and SR crossings of the latitude zone. Figure 3 shows the 13-yr average
169 distribution of those mean SS minus SR differences. They have vertical wavelengths and phase

170 changes as a function of latitude and pressure-altitude that are analogous to those for the diurnal
171 and/or semi-diurnal temperature tides (e.g., Andrews et al., 1987).

172

173 The two example time series of SS and SR points are in Figure 4 for the $22.5 \pm 7.5^\circ\text{S}$ latitude bin
174 at the 0.5-hPa and 2-hPa levels, and they are fitted using MLR methods. Note that the scaling of
175 the ordinate reverses for 0.5 hPa versus for 2.0 hPa to aid with visualizing the seasonal
176 temperature cycling both above and below the stratopause. Terms for the MLR model are
177 periodic annual (AO), semi-annual (SAO), and 853-day (~ 28 -mo) or quasi-biennial (QBO-like)
178 cycles. Remsberg (2008a) also included a 640-day (~ 21 -mo), sub-biennial term that represents
179 the difference frequency between the AO and QBO terms; that term has only small amplitude in
180 the uppermost stratosphere and lower mesosphere and is not included here. The regression
181 model also includes a normalized, Lyman- α (Lya) solar flux proxy term, a term to represent
182 ENSO forcings based on the MEI proxy series, and a linear (Lin) trend term; details of the
183 application of the two proxy terms to temperature and H₂O throughout the mesosphere are in
184 Remsberg et al. (2018). The normalized Lyman- α data have an 81-day smoothing applied to
185 them, to minimize the effect of flux variations from the 27-day solar rotation cycle. The HALOE
186 time series data are not de-seasonalized; instead, the model fit gives realistic estimates of
187 uncertainty by considering all terms at the same time. The grouping of HALOE profiles into 15°
188 or 20° -wide latitude bins provides adequate fittings for the seasonal as well as the longer-period
189 and proxy terms. Each model term also contains an adjustment for autocorrelation effects at lag-
190 1 (AR1) by the two-step approach of Cochrane & Orcutt (1949).

191

192 The MLR analyses begin in January 1993, even though Figure 4 shows HALOE data points from
193 late 1991 onward. Terms of the regression model constitute the oscillating curve, and they are at
194 bottom left. The straight line is just the sum of the constant and linear trend terms, as in Figure
195 2. Note that the amplitudes and interactions of the SAO and AO terms differ somewhat between
196 0.5 to 2 hPa; HALOE resolves them. Amplitudes of the QBO-like terms are only of order 1 K or
197 less and occur mainly at subtropical latitudes. Forcings from ENSO are not very significant
198 either, in agreement with findings from the regression analyses of Seidel et al. (2016). Figure 5
199 is the MLR analysis residuals from the fit at the 2-hPa level of Figure 4. There is no indication
200 of a volcanic perturbation early in 1993 in Figure 5, nor any remaining, periodic structures.

201

202 Table 1 (at top) contains numerical results from HALOE at 2 hPa for each of the latitude zones.
203 Temperature responses to the max-minus-min, Lyman-alpha (Lya) flux are in terms of degrees
204 K. Those responses are mostly positive or in-phase, as expected from photochemical modeling
205 studies (e.g., Marsh et al., 2007). Confidence intervals (CI in %) indicate the degree to which
206 Lya terms are present in the data. Responses are significant and of order 0.7 to 1.0 K across the
207 tropics and in the southern subtropics. They are near zero to slightly negative and not significant
208 at high latitudes. The analyzed HALOE T(p) response values agree with those from SABER at
209 50 km, which are of the order of 1 K in the tropics and then changing to zero or negative near
210 40° latitude (Huang et al., 2016, their Figure A1).

211

212 The HALOE trend terms in Table 1 have units of K/decade, and they are essentially orthogonal
213 to the solar flux terms. There is a significant cooling of the order of -1.0 K/decade at low

214 latitudes, which is about twice that from SABER data for the later period of 2002-2012 (Huang
215 et al., 2014, their Figure 2). Note that both data analyses are for time spans, when major
216 volcanic eruptions and their possible forcing effects should not be a concern. The temperature
217 trend differences between HALOE and SABER indicate the effect of changing ODS forcings on
218 ozone. ODS was leveling off during the HALOE period, such that most of the observed total
219 atmospheric cooling ought to be due to the steadily increasing CO₂. The SABER T(p) trends are
220 for the following decade, when ODS was in decline and ozone was starting to increase at middle
221 latitudes (see also Figure 2 of Huang et al., 2014).

222

223 **4. T(p) trends from HALOE and from SSU3**

224 Figure 6 shows the distribution of temperature trends from HALOE along with estimates of their
225 uncertainty (CI values in %). The HALOE trends at 2.0 hPa are those given in Table 1; they are
226 significant and vary smoothly with latitude. The trends at 3.0 hPa also vary smoothly and are
227 even more negative (-1.5 K/decade). It is likely that they carry a negative bias due to the
228 merging of the HALOE and CPC profiles at lower altitudes (see Figure 2). On the other hand,
229 there is a clear hemispheric asymmetry in the T(p) trends at 1.0 and 0.7 hPa, where values are
230 negative and significant in the subtropics of the SH but not the NH (zero to slightly positive).
231 No similar asymmetry is present in the trend pattern from the SABER data (Huang et al., 2014).
232 Such differences imply that the forcings from ODS, GHG, and/or from the effects of wave
233 activity are not the same for the two hemispheres during the time of HALOE.

234

235 Figures 7 and 8 provide a qualitative check on the HALOE temperature trends in the upper
236 stratosphere for 1993-2005. Figure 7 is an analysis of the merged SSU3 time series for the 15°-
237 wide latitude bin centered at 22°S and based on zonal-averages of its gridded data obtained from
238 the NOAA/STAR Website. Note that the SSU temperatures already include adjustments to
239 account for changes in atmospheric CO₂ and in the CO₂ gas cell content over time (Wang et al.,
240 2012). Merged SSU3 data also include adjustments for time-of-day differences of the
241 observations from successive satellite sensors, and they have a time tag of 1200 LT (Zou & Qian,
242 2016). The mean of the SSU3 temperature time series at 22°S is 248.9 K or colder by about 10
243 K compared to the mean of the HALOE time series at 2.0 hPa (Figure 4). The primary reason
244 for the difference is that the measured radiances for SSU3 and for AMSU-A channel 14 extend
245 lower in the stratosphere.

246

247 Numerical results from SSU3 with latitude are also in Table 1 (at bottom). Their T(p) responses
248 to the max-minus-min solar flux proxy are about 0.5 K and significant, and their trends at the
249 lower latitudes are between -0.2 and -0.5 K/decade. SSU3 has lower vertical resolution, and its
250 mean temperature values vary from 244 K to 249 K from high to low latitudes; those values are
251 also cooler by about 4 K than the ones from HALOE at 3.0 hPa. Nevertheless, 2.5 hPa is set as
252 the pressure altitude of the analyzed SSU3 temperature trends, based on an estimate of their
253 combined contribution functions. Clearly, a disadvantage of T(p) time series from the current
254 operational sounders is that they do not resolve changes in the trends across the stratopause.

255

256 Figure 8 compares the trends from Table 1 for SSU3 and HALOE. Note that the trends from
257 both are not as significant at the higher latitudes, where the seasonal amplitudes are large.
258 Analyzed trends for SSU3 at 22°S carry an uncertainty (the tiny vertical bar) of only about ±0.05
259 K/decade (2σ), which is similar to the error estimates of Zou and Qian (2016, their Figure 9)
260 after taking averages of the SSU3 data over six adjacent 2.5° latitude bins as done here. On the
261 other hand, the similar error estimates for the HALOE trends are really an underestimate because
262 they do not account for the fact that the HALOE time series points only approximate a true zonal
263 mean, particularly at the higher latitudes in winter when the zonal variations are large. For
264 instance, the two separate HALOE curves in Figure 8 are for its trends based on averages of
265 more than five profiles versus more than seven profiles for each given bin. In addition, the
266 HALOE profiles do not always sample each latitude bin uniformly. Thus, the trend differences
267 between those two HALOE curves are a better measure of their T(p) uncertainties.

268

269 Figure 9 shows the two hemispheric, HALOE temperature trend profiles from 0.3 to 3.0 hPa.
270 They are the result of applying an area-weighting calculation to the separate T(p) trends across
271 their four latitudes zones and then normalizing them by the area of the hemisphere, where the
272 area north of a line of latitude is defined as

$$273 \quad A = 2 \pi R^2 (1 - \sin(\text{lat})) \quad (1)$$

274 and R is Earth's radius. As an example, the normalized area of the zone between 15° and 30° is
275 0.241. Horizontal bars denote the range of the trends within each hemisphere for a level. The
276 southern hemisphere trend profile is negative and significant, while the northern hemisphere

277 trends are effectively zero across the stratopause. The next two sections consider whether any of
278 the forcings are also different for the two hemispheres.

279

280 The near-global HALOE trend profile in Figure 9 is simply an average across both hemispheres,
281 and it is clearly different from the calculated total temperature trend profile adopted from Shine
282 et al. (2003). HALOE $T(p)$ shows a minimal cooling of -0.2 K/decade at 1 hPa, as opposed to
283 the maximum radiative response of Figure 1 for GHG and for ozone when ODS was increasing
284 in 1980-2000. These differences agree qualitatively with the conclusion of Aquila et al. (2016)
285 that changing from a negative to a slightly positive ozone trend is the primary radiative forcing
286 agent for the corresponding changes in global temperature trends from 1979-1997 to 2000-2011.

287

288 Figure 9 also includes the area-weighted, global trend from SSU3 (-0.3 K/decade) for 1993-
289 2005, and it compares most closely with the HALOE trend at 1.5 hPa. The trend from SSU3 is
290 smaller than the trends of -0.7 to -0.8 K/decade of Zou & Qian (2013) and of -0.5 to -0.6
291 K/decade of Randel et al. (2016) for their longer time spans of 1979-2015. However, it is
292 identical to the value of Randel et al. (2016) for their shorter period of 1998-2015. Further, it is
293 likely that the near-global HALOE $T(p)$ trend in Figure 9 at 3 hPa has a negative bias and is not
294 representative; analyzed trends at 3 hPa are omitted from here on.

295

296 **5. Estimates of trend attribution using HALOE data**

297 Remsberg (2008b) reported on ozone trends from HALOE that are near zero in the upper
298 stratosphere, although he employed a simple 11-yr sinusoid rather than a solar flux proxy time
299 series to account for concurrent solar forcing effects. He also showed that there was little change
300 in his MLR ozone trends, when he considered a time series proxy for the ODS rather than a
301 linear trend in his ozone modeling. That insensitivity to the exact nature of the ODS trends is
302 because they are small during 1993-2005. Figure 10 shows updated ozone analysis results, based
303 on the current latitude bins and regression model terms (including the proxy L_{ya} solar term) for
304 1993-2005. The ozone trends in Figure 10 are slightly positive near the stratopause across the
305 low and middle latitudes. However, there is no clear hemispheric asymmetry for the trends,
306 presumably because ozone is under photochemical control at that altitude. Regions of dark
307 shading show that the ozone trends in the middle stratosphere are negative and significant at the
308 95% confidence interval (CI), most notably at middle latitudes of the southern hemisphere. The
309 reduced significance of the trends in the northern hemisphere indicate effects of wintertime
310 mixing just below the region of transition from photochemical to dynamical control for the
311 stratospheric ozone distribution (Leovy et al. 1985).

312

313 One can be more confident that the ozone trends in Figure 10 are representative by examining
314 the distribution in Figure 11 of the associated MLR responses of the ozone time series to the
315 maximum minus minimum solar flux forcing during those years. That ozone response
316 distribution extends through most of the stratosphere. It is of order 2 to 3% and highly
317 significant in the middle to upper stratosphere at middle latitudes. Figure 12 is the average
318 response profile across 30°S to 30°N latitude, along with a representative model profile of the
319 response to the solar cycle uv-flux variations at 5°N from Brasseur (1993).

320

321 Radiative effects from CO₂ comprise almost all of the GHG forcings, and CO₂ had an average
322 growth rate of 1.5 ppmv/yr in the 1990s compared with only slightly larger values in the 1980s
323 and the early 2000s (WMO, 2011). Trends in the secondary radiative forcing agent H₂O were
324 near zero in the lowermost mesosphere at this time (not shown, but see Remsberg et al., 2018;
325 Nedoluha et al., 2017; Scherer et al., 2008), such that there is little to no H₂O cooling
326 contributing to the analyzed HALOE T(p) trend profile.

327

328 Attribution of radiative heating/cooling to GHG, ozone, and H₂O is in following manner. There
329 are adjustments made to the fixed dynamical heating (FDH) calculations of Shine et al. (2003),
330 according to the HALOE gas trends for 1993-2005. First, the HALOE GHG (CO₂) cooling
331 profile is set the same as that from Shine et al. On the other hand, the ozone trends from
332 HALOE are much smaller than those from the Stratospheric Aerosol and Gas Experiment
333 (SAGE) of Randel & Wu (1999) used by Shine et al. (2003). Thus, the ozone heating rates for
334 the HALOE period are from a scaling of the ozone heating rate profile of Shine et al. (2003) by
335 the ratio of the HALOE and SAGE average ozone trend profiles for their respective time spans.
336 Further, the SAGE ozone distributions of Randel and Wu (1999) extend from about 60°S to
337 60°N, which is nearly the same latitude range as the ozone trends from the HALOE data.
338 Similarly, the heating rate profile for H₂O has a scaling by the ratio of HALOE H₂O trend
339 distribution to the constant H₂O profile of 1 %/decade considered in Shine et al. (2003). Table 2
340 contains the near-global, trend profile estimates for ozone and H₂O from Shine et al. (2003)
341 along with the ones analyzed here from the HALOE data. Finally, the scaled, area-weighted

342 heating rate profiles for HALOE are in Table 3, keeping in mind that the HALOE ozone and
343 H₂O heating profiles are not quite global (lacking the area poleward of 65° latitude or by 10% of
344 total area). Table 3 also has the HALOE total heating rate profile—a sum of ones for the GHG,
345 ozone, and H₂O.

346
347 Figure 13 compares that estimated near-global, total heating rate profile (+ signs) with the
348 analyzed HALOE temperature trend profile from Figure 9 (asterisks), and their overall values
349 agree closely. The separate gas contributions to the HALOE heating/cooling rates are also in
350 Figure 13; compare them with those for 1980-2000 shown in Figure 1, as adopted from Shine et
351 al. (2003). The primary difference for the temperature trends comes from the changes in ozone
352 over that time span. The HALOE temperature trends are also similar to the modeled effects of
353 the radiative forcings in Checa-Garcia et al. (2018, their Figure 2), which show a near zero
354 temperature trend at the stratopause due to changes in ozone between the 1990s and the 2000s.

355

356 **6. Attribution of hemispheric differences in temperature trends**

357 The minimum, near-global HALOE temperature trend of -0.2 K/decade at 1 hPa in Figure 13 is
358 not matched by a corresponding minimum in the total cooling profile. That difference occurs at
359 the level where there is a clear change in Figure 6 from negative to slightly positive HALOE
360 temperature trends between the two hemispheres. Yet, there are no clear indications of
361 hemispheric differences in the trends from the radiatively-active gases. It may be that the upper
362 stratosphere and lower mesosphere experienced trends in the diabatic circulation or the closely-
363 related, mean residual circulation (MRC) due to forcings from the dissipation of planetary

364 waves, particularly when the zonal wind regime is westerly or from late autumn to early spring
365 (e.g., Linz et al., 2018; Langematz et al., 2003). Examination of trends for a dynamical tracer
366 may indicate whether such activity is important for the HALOE temperature time series.

367

368 The chemical time constant for CH₄ increases from a minimum of about three months at 2.0 hPa
369 to six months at 0.5 hPa, or longer than typical net transport times (Brasseur & Solomon, 2005).
370 In fact, Fleming et al. (1999) used the monthly HALOE CH₄ distributions, as effective tracers of
371 the seasonal circulations for diagnosing the net transport in zonally-averaged models. HALOE
372 data indicate an upwelling of CH₄ to above the stratopause at subtropical latitudes from autumn
373 to springtime. CH₄ also responds to a secondary tropical circulation associated with the descent
374 of the SAO wind regime. Remsberg (2015) reported on initial analyses of HALOE CH₄ in an
375 attempt to diagnose its longer-term changes due to wave-induced, net circulations. He found
376 anti-correlations of the changes in CH₄ versus those of H₂O, as expected, since CH₄ oxidizes to
377 form H₂O in the upper stratosphere. CH₄ also has anti-correlations with HCl—a species having
378 vertical and horizontal gradients opposite those of CH₄.

379

380 Trends for CH₄ in the troposphere are variable but of the order of 2 to 3 %/decade during the
381 time of HALOE (Dlugokencky et al., 2009; Solomon et al., 2007). Remsberg (2015, his Figure
382 7) reported tropical trends from HALOE of the same order for the lowermost stratosphere (50
383 hPa). Figure 14 is an update of the stratospheric distribution of his analyzed trends for HALOE
384 CH₄ along with estimates of their significance. The data for Figure 14 are restricted to between

385 65°N/S, and the MLR modeling is for the same time span as for temperature, ozone and H₂O and
386 uses the same periodic terms, plus the solar and MEI proxy terms.

387

388 There is good continuity with latitude and altitude for the trends in Figure 14 from the MLR
389 analyses of the set of 96 separate time series. CH₄ trends at the 10-hPa level and extending to the
390 lower mesosphere are larger (4 to 8 %/decade at low to middle latitudes) than those of the
391 troposphere and tropical lower stratosphere (~2 %/decade). Increasing CH₄ trends from the
392 lower to the middle tropical stratosphere imply that there was acceleration from the lower branch
393 of the Brewer-Dobson circulation (BDC) during the years of the HALOE observations, and this
394 finding is consistent with age-of-air estimates from atmospheric re-analyses for 1989 to 2010
395 (Diallo et al., 2012, Figure 13). CH₄ trends are nearly constant in the upper stratosphere and of
396 the order of 8 %/decade across tropical and subtropical latitudes of both hemispheres. Notably
397 though, the trends across the stratopause are more significant for the 22.5° zone of the southern
398 than the northern hemisphere.

399

400 Figure 15 shows time series of HALOE CH₄ at 2.0 hPa for both the subtropics of the northern
401 and the southern hemispheres. The seasonal cycle (AO and SAO) dominates CH₄ in the southern
402 subtropics, while the influence of the QBO-like oscillation is evident in the northern subtropics.
403 It is also apparent that the seasonal terms of the MLR model do not match the data as well most
404 years in the northern hemisphere, giving rise to the lower significance for the fit of all terms
405 including the trends. One caution about the MLR modeling of CH₄ is that its trend terms at the
406 higher altitudes are sensitive to endpoint anomalies in the time series. For instance, when the

407 analyses begin at January 1992 instead of 1993, there is an influence from the relatively high
408 CH₄ values of 1992 such that the derived trends become much smaller than shown in Figure 15.
409 Therefore, the most robust result for the stratopause region from Figures 14 and 15 is that the
410 CH₄ trends are significant in the southern but not the northern hemisphere.

411

412 The current MLR modeling includes one term related to wave-induced effects, the ENSO index
413 proxy. However, it does not account for the episodic forcings related to sudden stratospheric
414 warmings (SSW) activity, which is prevalent in the northern but not the southern hemisphere
415 most winters (Remsberg, 2015). Dissipation of the propagating planetary waves at those times
416 impart a heating to the stratopause region at high latitudes, and there follows a compensating,
417 meridional exchange of air between high and low latitudes (Langematz et al., 2003). Charlton
418 and Polvani (2007) reported that major SSWs were absent from 1990 through 1997, but then
419 occurred every year from 1998 through 2002. Because the HALOE analyses extend from 1993
420 to 2005, it may be that the pattern of hemispheric temperature trends in Figure 6 reflect a lack of
421 and then the reoccurrence of wintertime wave activity and SSWs during 1993-2005. An
422 additional proxy term is missing for the representation of such episodic wave forcings in the
423 present MLR modeling. While it may be possible to account for their effects using atmospheric
424 reanalysis data, that effort is beyond the scope of this study.

425

426 **7. Conclusions**

427 Analyses of time series of HALOE profile data reveal the trends in temperature in the region of
428 the stratopause (from 2.0 to 0.5 hPa) for 1993-2005. The HALOE trends at 2.0 hPa are of the

429 order of -1.0 K/decade across the tropics and subtropics, but then become smaller (-0.5
430 K/decade) at the middle latitudes. The near-global HALOE trend at 1.5 hPa is similar to that
431 from merged SSU3 operational data, although the two results are not strictly for the same altitude
432 region. The near-global HALOE trend profile has a minimum cooling rate of -0.2 K/decade at
433 1.0 hPa, but with a range of -0.6 K/decade for the southern hemisphere to 0.2 K/decade in the
434 northern hemisphere.

435

436 Analyses for the concurrent trends in HALOE ozone and H₂O provide estimates of their
437 contributions to the radiative heating/cooling in that region. In particular, the trends in upper
438 stratospheric ozone during the time of HALOE are zero to weakly positive, leading to a slight
439 warming. Upon combining the forcings from ozone and H₂O with estimates of the concurrent
440 cooling from the steadily increasing CO₂, there is a near-global total cooling trend of -0.5
441 K/decade across the stratopause that is nearly symmetric across the two hemispheres. Both the
442 HALOE temperature trend and total radiative cooling profiles differ from those reported from
443 observations and calculations for 1980-2000, mainly because the ozone trends changed from
444 clearly negative in the 1980s through mid-1990s to slightly positive during the time of HALOE.

445

446 Trends in HALOE CH₄, a tracer-like molecule, increase from about 2 to more than 4 %/decade
447 from 50 hPa to above 10 hPa, suggesting that there was an acceleration of the Brewer/Dobson
448 circulation during 1993-2005. The trends for HALOE temperature and CH₄ in the region of the
449 stratopause are significant only in the southern hemisphere. The CH₄ time series of the northern
450 hemisphere reveal non-periodic, subseasonal variability, especially during and following SSW

451 events. Because major wintertime warmings were absent from 1993 through 1997, it may be
452 that there is a trend in the wave activity and its effect on temperature that is specific to the years
453 of the analyses herein (1993-2005). The present results from HALOE demonstrate that relatively
454 high, vertical resolution measurements, like those from MLS and SABER, should also be able to
455 provide trends in temperature across the stratopause as well as estimates of contributions to them
456 based on their retrieved profiles of the primary, radiative forcing agents.

457

458 **Acknowledgements.** HALOE data are from (<http://haloe.gats-inc.com/home/index.php/>), daily
459 Ly- α fluxes are from (<http://lasp.colorado.edu/lisird/lya/>), and ENSO MEI values are from
460 (<https://www.esrl.noaa.gov/psd/enso/mei/>). Trends in tropospheric methane are from
461 NOAA/ESRL (www.esrl.noaa.gov/gmd/ccgg/trends_ch4/). Gridded and merged SSU3/AMSU-
462 A, Version 3.0 data are available from NOAA STAR via
463 [ftp://ftp.star.nesdis.noaa.gov/pub/smcd/emb/mscat/data/SSU/SSU_v3.0/SSU_AMSU_Monthly_Layer_Tem](ftp://ftp.star.nesdis.noaa.gov/pub/smcd/emb/mscat/data/SSU/SSU_v3.0/SSU_AMSU_Monthly_Layer_Temperature/)
464 [perature/](ftp://ftp.star.nesdis.noaa.gov/pub/smcd/emb/mscat/data/SSU/SSU_v3.0/SSU_AMSU_Monthly_Layer_Temperature/). ER acknowledges Cheng-Zhi Zou of NOAA/NESDIS for his comments about the
465 operational temperature data. Larry Gordley directed the study of possible instrument effects in
466 the trends from the HALOE radiometer channels (for CO₂, ozone, and H₂O), a critical part of the
467 findings herein. ER performed this study as a Distinguished Research Associate (DRA) at
468 NASA Langley, and he has no competing interests for the work.

469

470 **References**

471 Andrews, D. G., Holton, J. R., & Leovy, C. B. (1987). *Middle atmosphere dynamics* (489 pp.).
472 Orlando, FL: Academic Press, Inc.

473

474 Aquila, V., Swartz, W. H., Waugh, D. W., Colarco, P. R., Pawson, S., Polvani, L. M., &
475 Stolarski, R. S. (2016). Isolating the roles of different forcing agents in global stratospheric
476 temperature changes using model integrations with incrementally added single forcings. *J.*
477 *Geophys. Res.*, *121*, 8067-8082, doi:10.1029/2015JD023841

478

479 Brasseur, G. (1993). The response of the middle atmosphere to long-term and short-term solar
480 variability: a two-dimensional model. *J. Geophys. Res.*, *98*, 23079-23090,
481 doi:10.1029/93JD02406

482

483 Brasseur, G., & Solomon, S. (2005). *Aeronomy of the middle atmosphere*, 3rd Edition, in
484 Atmospheric and Oceanographic Sciences Library, Vol. 32, Springer, the Netherlands, 664 pp.

485

486 Charlton, A. D., and L. M. Polvani (2007). A new look at stratospheric sudden warmings. Part I:
487 climatology and modeling benchmarks. *J. Climate*, *20*, 449-469,
488 <https://doi.org/10.1175/JCLI3996.1>

489 Checa-Garcia, R., Hegglin, M. I., Kinnison, D., Plummer, D. A., & Shine, K. P. (2018).
490 Historical tropospheric and stratospheric ozone radiative forcing using the CMIP6 database.
491 *Geophys. Res. Lett.* *45*, <https://doi.org/10.1002/2017GL076720>
492

493 Cochran, D., & Orcutt, G. (1949). Application of least squares regression to relationships
494 containing auto-correlated error terms. *Journal of the American Statistical Association*, *44*(245),
495 32-61. <https://doi.org/10.1080/0162459.1949.10483290>
496

497 Diallo, M., Legras, B., & Chedin, A. (2012). Age of stratospheric air in the ERA-Interim.
498 *Atmos. Chem. Phys.*, *12*, 12133-12154, doi:10.5194/acp-12-12133-2012
499

500 Dlugokencky, E. J. & Co-authors (2009). Observational constraints on recent increases in the
501 atmospheric CH₄ burden. *Geophys. Res. Lett.*, *36*, L18803, doi:10.1029/2009GL039780
502

503 Fleming, E. L., Jackman, C. H., Stolarski, R. S., & Considine, D. B. (1999). Simulation of
504 stratospheric tracers using an improved empirically based two-dimensional model transport
505 formulation. *J. Geophys. Res.*, *104*, 23911-23934
506

507 Garcia, R. R., Marsh, D. R., Kinnison, D. E., Boville, B. A., & Sassi, F. (2007). Simulation of
508 secular trends in the middle atmosphere, 1950-2003. *J. Geophys. Res.*, *112*, D09301,
509 doi:10.1029/2006JD007485

510

511 Gordley, L. L., Thompson, E., McHugh, M., Remsberg, E., Russell III, J., & Magill, B. (2009).
512 Accuracy of atmospheric trends inferred from the halogen occultation experiment. *J. Appl.*
513 *Remote Sens.*, *3*, 033526, doi:10.1117/1.3131722

514

515 Huang, F. T., Mayr, H. G., Russell III, J. M., & Mlynczak, M. G. (2016). Ozone and
516 temperature decadal responses to solar variability in the mesosphere and lower thermosphere,
517 based on measurements from SABER on TIMED. *Ann. Geophys.*, *34*, 29-40, doi:10.5194/angeo-
518 34-29-2016

519

520 Huang, F. T., Mayr, H. G., Russell III, J. M., & Mlynczak, M. G. (2014). Ozone and temperature
521 decadal trends in the stratosphere, mesosphere and lower thermosphere, based on measurements
522 from SABER on TIMED. *Ann. Geophys.*, *32*, 935-949, doi:10.5194/angeo-32-935-2014

523

524 Langematz, U., Kunze, M., Kreuger, K., & Labitzke, K. (2003). Thermal and dynamical changes
525 of the stratosphere since 1979 and their link to ozone and CO₂ changes. *J. Geophys. Res.*, *108*,
526 D1, 4027, doi:10.1029/2002JD002069

527

528 Lee, H., & Smith, A. K. (2003). Simulation of the combined effects of solar cycle, quasi-
529 biennial oscillation, and volcanic forcing on stratospheric ozone changes in recent decades. *J.*
530 *Geophys. Res.*, 108, D2, 4049, doi:10.1029/2001JD001503
531

532 Leovy, C. B., Sun, C-R., Hitchman, M. H., Remsberg, E. E., Russell III, J. M., Gordley, L. L.,
533 Gille, J. C., and Lyjak, L. V. (1985). Transport of ozone in the middle stratosphere: evidence for
534 planetary wave breaking. *J. Atmos. Sci.*, 42, 230-244, [https://doi.org/10.1175/1520-
535 0469\(1985\)042%3C0230:TOOITM%3E2.0.CO;2](https://doi.org/10.1175/1520-0469(1985)042%3C0230:TOOITM%3E2.0.CO;2)
536

537 Linz, M., Abalos, M., Glanville, A. S., Kinnison, D. E., Ming, A., and Neu, J. (2018). The
538 global overturning diabatic circulation of the stratosphere as a metric for the Brewer-Dobson
539 circulation. *Atmos. Chem. Phys. Discuss.*, <https://doi.org/10.5194/acp-2018-972>
540

541 Marsh, D. R., Garcia, R. R., Kinnison, D. E., Boville, B. A., Sassi, F., Solomon, S. C., and
542 Matthes, K. (2007). Modeling the whole atmosphere response to solar cycle changes in radiative
543 and geomagnetic forcing. *J. Geophys. Res.*, 112, D23306, doi:10.1029/2006JD008306
544

545 Maycock, A. C., & Coauthors (2018). Revisiting the mystery of recent stratospheric temperature
546 trends, *Geophys. Res. Lett.*, 45, <https://doi.org/10.1029/2018GL078035>
547

548 McLandress, C., Shepherd, T. G., Jonsson, A. I., von Clarmann, T., & Funke, B. (2015). A
549 method for merging nadir-sounding climate records, with an application to the global-mean
550 stratospheric temperature data sets from SSU and AMSU. *Atmos. Chem. Phys.*, *15*, 9271-9284,
551 doi:10.5194/acp-15-9271-2015

552

553 Nash, J., & Saunders, R. (2015). A review of stratospheric sounding unit radiance observations
554 for climate trends and reanalyses, *Q. J. R. Meteorol. Soc.*, *141*, 2103-2113, doi:10.1002/qj.2505

555

556 Nedoluha, G. E., & Coauthors (2017). The SPARC water vapor assessment II: intercomparison
557 of satellite and ground-based microwave measurements. *Atmos. Chem. Phys.*, *17*, 14543-14558,
558 <https://doi.org/10.5194/acp-17-14543-2017>.

559

560 Ramaswamy, V., & Coauthors (2001). Stratospheric temperature trends: observations and model
561 simulations. *Rev. Geophys.*, *39*, 71-122, doi:10.1029/1999RG000065.

562

563 Randel, W. J., & Wu, F. (1999). A stratospheric ozone trends data set for global modeling
564 studies. *Geophys. Res. Lett.*, *26*, 3089-3092, <https://doi.org/10.1029/1999GL900615>

565

566 Randel, W. J., Smith, A. K., Wu, F., Zou, C-Z., & Qian, H. (2016) Stratospheric temperature
567 trends over 1979-2015 derived from combined SSU, MLS, and SABER satellite observations. *J.*
568 *Climate*, 29, 4843-4859, doi:10.1175/JCLI-D-15-0629.1

569

570 Randel, W. J., and Coauthors (2009). An update of observed stratospheric temperature trends. *J.*
571 *Geophys. Res.*, 114, D02107, doi:10.1029/2008JD010421

572

573 Remsberg, E. E. (2008a). On the observed changes in upper stratospheric and mesospheric
574 temperatures from UARS HALOE. *Ann. Geophys.*, 26, 1287-1297, [www.ann-](http://www.ann-geophys.net/26/1287/2008/)
575 [geophys.net/26/1287/2008/](http://www.ann-geophys.net/26/1287/2008/)

576

577 Remsberg, E. (2008b). On the response of Halogen Occultation Experiment (HALOE)
578 stratospheric ozone and temperature to the 11-year solar cycle forcing. *J. Geophys. Res.*, 113,
579 D22304, doi:10.1029/2008JD010189

580

581 Remsberg, E. E. (2015). Methane as a diagnostic tracer of changes in the Brewer-Dobson
582 circulation of the stratosphere. *Atmos. Chem. Phys.*, 15, 3739-3754, doi:10.5194/acp-15-3739-
583 2015

584

585 Remsberg, E. E., & Deaver, L. E. (2005). Interannual, solar cycle, and trend terms in middle
586 atmospheric temperature time series from HALOE. *J. Geophys. Res.*, *110*, D06106,
587 doi:10.1029/2004JD004905

588

589 Remsberg, E. E., & Coauthors (2002). An assessment of the quality of Halogen Occultation
590 Experiment temperature profiles in the mesosphere based on comparisons with Rayleigh
591 backscatter lidar and inflatable falling sphere measurements. *J. Geophys. Res.*, *107*, D20, 4447,
592 doi:10.1029/2001JD001521

593

594 Remsberg, E., Damadeo, R., Natarajan, M., & Bhatt, P. (2018). Observed responses of
595 mesospheric water vapor to solar cycle and dynamical forcings. *J. Geophys. Res.*, *123*, 3830-
596 3843, <https://doi.org/10.1002/2017JD028029>

597

598 Rosenlof, K. H., & Coauthors (2001). Stratospheric water vapor increases over the past half-
599 century. *Geophys. Res. Lett.*, *28*, 1195-1198, doi:10.1029/2000GL012502

600

601 Russell III, J. M., & Coauthors (1993). The Halogen Occultation Experiment. *J. Geophys. Res.*,
602 *98*, 10777-10798, <https://doi.org/10.1029/93JD00799>

603

604 Scherer, M., Voemel, H., Fueglistaler, S., Oltmans, S. J., & Staehelin, J. (2008). Trends and
605 variability of midlatitude stratospheric water vapour deduced from the re-evaluated Boulder
606 balloon series and HALOE. *Atmos. Chem. Phys.*, 8, 1391-1402, [www.atmos-chem-](http://www.atmos-chem-phys.net/8/1391/2008/)
607 [phys.net/8/1391/2008/](http://www.atmos-chem-phys.net/8/1391/2008/)
608

609 Seidel, D. J., & Coauthors (2016). Stratospheric temperature changes during the satellite era. *J.*
610 *Geophys. Res.*, 121, 664-681, doi:10.1002/2015JD024039
611

612 Shine, K. P., & Coauthors (2003). A comparison of model-simulation trends in stratospheric
613 temperatures. *Q. J. R. Meteorol. Soc.*, 129, 1565-1588, doi:10.1256/qj.02.186
614

615 Solomon, S., Qin, D., Manning, M., Chen, Z., Marquis, M., Averyt, K. B., Tignor, M., and
616 Miller, H. L. (eds.), *Contribution of Working Group I to the Fourth Assessment Report (AR4) of*
617 *the Intergovernmental Panel on Climate Change (IPCC), 2007*, 996 pp., Cambridge University
618 Press, New York, USA
619

620 Stolarski, R. S., Douglass, A. R., Newman, P. A., Pawson, S., & Schoeberl, M. R. (2010)
621 Relative contribution of greenhouse gases and ozone-depleting substances to temperature trends
622 in the stratosphere: a chemistry-climate model study. *J. Climate*, 23, 28-42,
623 doi:10.1175/2009KC:O2955.1

624

625 Thompson, R. E., & Gordley, L. L. (2009). Retrieval algorithms for the Halogen Occultation
626 Experiment. *NASA/Contractor Report 2009-215761*. 106 pp. Available from NASA CASI,
627 Hanover, MD

628

629 Wang, L., Zou, C-Z., & Qian, H. (2012). Construction of stratospheric temperature data records
630 from Stratospheric Sounding Units. *J. Climate*, 25, 2931-2946, doi:10.1175/JCLI-D-11-00350.1

631

632 WMO (2011). *Scientific Assessment of Ozone Depletion: 2010*, Global Ozone Research and
633 Monitoring Project—Report No. 52, 516 pp., Geneva, Switzerland

634

635 Zou, C.-Z., & Qian, H. (2016). Stratospheric temperature climate data record from merged SSU
636 and AMSU-A observations. *J. Atmos. Oceanic Tech.*, 33, 1967-1984, doi:10.1175/JTECH-D-16-
637 0018.1

638

639

Latitude	55S	37.5S	22.7S	7.5S	7.5N	22.5N	37.5N	55N
HALOE								
Lya	0.1	-1.4	0.7	1.0	1.0	0.3	1.0	-0.1
CI, %	10	78	90	94	95	72	79	1
Trend	-0.7	-0.3	-1.2	-1.1	-0.9	-0.9	-0.8	0.2
CI, %	54	16	99	90	86	98	79	11
SSU3								
Lya	0.0	0.1	0.5	0.6	0.5	0.5	0.8	0.3
CI, %	6	38	97	88	92	94	65	47
Trend	-0.2	-0.2	-0.5	-0.5	-0.3	-0.2	0.0	-0.7
CI, %	2	38	99	71	69	51	5	43

641

642 Table 1—Analyzed responses of temperature (K) to max-minus-min solar cycle fluxes (Lya) and
643 the linear trends (K/decade) in time series of T(p) from (top) HALOE at 2 hPa and from (bottom)
644 SSU3, as a function of latitude for 1993 to 2005. Confidence intervals (CI in %) denote the
645 likelihood that the two separate terms are present in the time series.

646

647

648

Pressure- altitude (hPa)	O3 Trends, 1980-2000 (%/decade)	H2O Trends, 1980-2000 (%/decade)	O3 Trends, HALOE (%/decade)	H2O Trend, HALOE (%/decade)
0.3	-2.0	+1.0	+0.67	+0.66
0.5	-2.0	+1.0	+0.63	+0.23
0.7	-3.0	+1.0	+0.57	-0.42
1.0	-4.0	+1.0	+0.50	-0.86
1.5	-5.0	+1.0	+0.49	-1.06
2.0	-6.0	+1.0	+0.50	-1.10
3.0	-7.0	+1.0	+0.37	-1.30

649

650 Table 2—Trend profiles of ozone and water vapor for 1980-2000 and for 1993-2005.

651

652

Pressure (hPa)	O3 heating from Shine (K/decade)	O3 heating HALOE (K/decade)	H2O heating from Shine (K/decade)	H2O heating HALOE (K/decade)	GHG heating, Shine & HALOE (K/decade)	Total heating HALOE (K/decade)
0.3	-0.40	+0.12	-0.2	-0.15	-0.50	-0.53
0.5	-0.65	+0.15	-0.2	-0.04	-0.75	-0.64
0.7	-0.85	+0.11	-0.2	+0.07	-0.80	-0.62
1.0	-0.95	+0.12	-0.2	+0.16	-0.80	-0.52
1.5	-0.83	+0.07	-0.2	+0.21	-0.75	-0.47
2.0	-0.70	+0.02	-0.2	+0.22	-0.70	-0.46
3.0	-0.40	+0.00	-0.2	+0.26	-0.60	-0.34

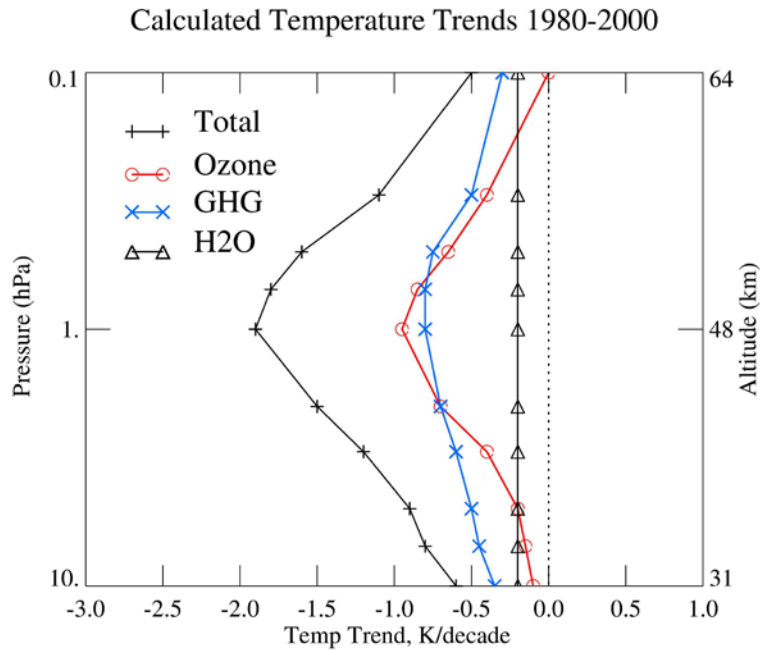
653

654 Table 3—Contributions to heating/cooling for GHG, O3, and H2O in Shine et al. (2003) and

655 from HALOE and total heating rate profile from HALOE (last column).

656

657

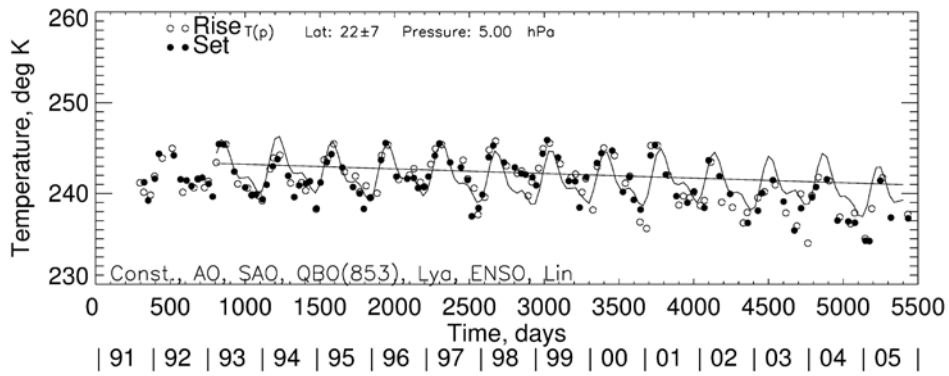


658

659 Figure 1—Total calculated temperature trends for 1980-2000, as adopted from Figure 5 of Shine
660 et al. (2003). Separate contributions are from the trends in ozone (red), in the greenhouse gases
661 (GHG in blue), and in H₂O.

662

663



664

665 Figure 2—Time series of HALOE T(p) at 5 hPa and 22.5°N latitude. Analyses are for 1993 and

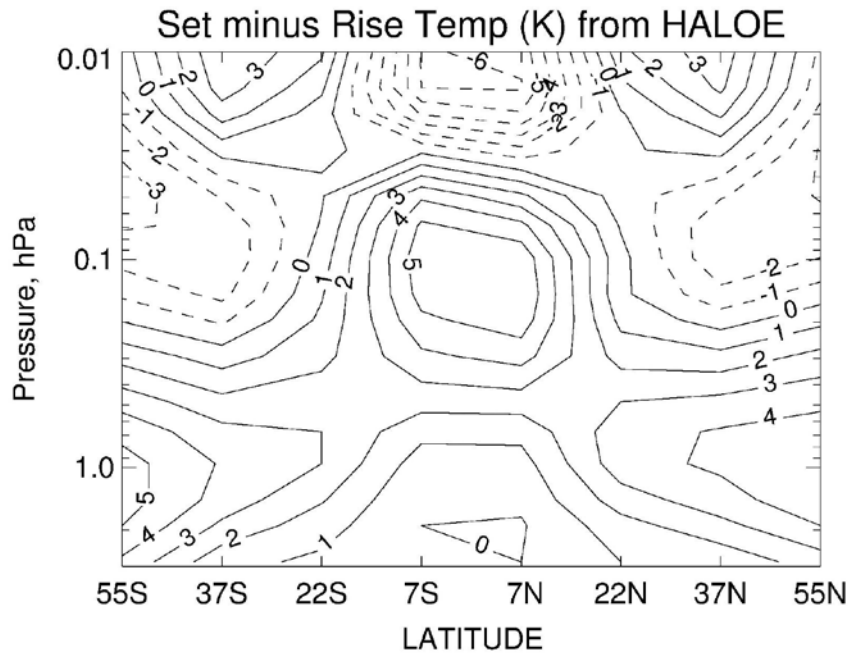
666 onward. Terms of the regression model are at bottom left and constitute the oscillating curve.

667 The straight line is a sum of the constant and linear trend terms.

668

669

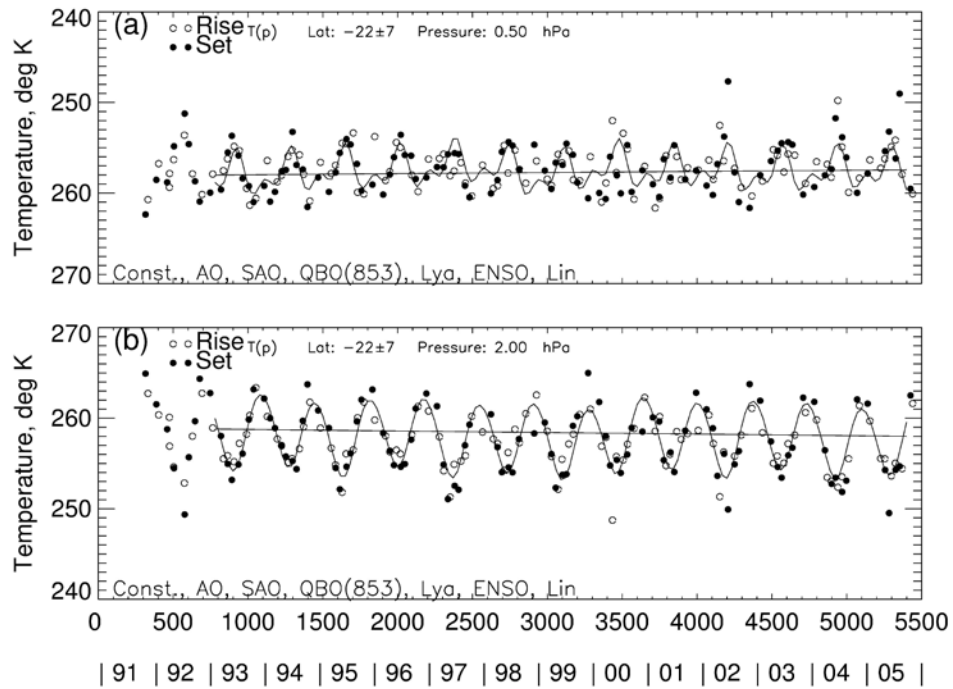
670



671

672 Figure 3—Distribution of average sunset (SS) minus sunrise (SR) temperatures (in K) from
673 HALOE for the upper stratosphere and mesosphere and from 1993 to 2005.

674

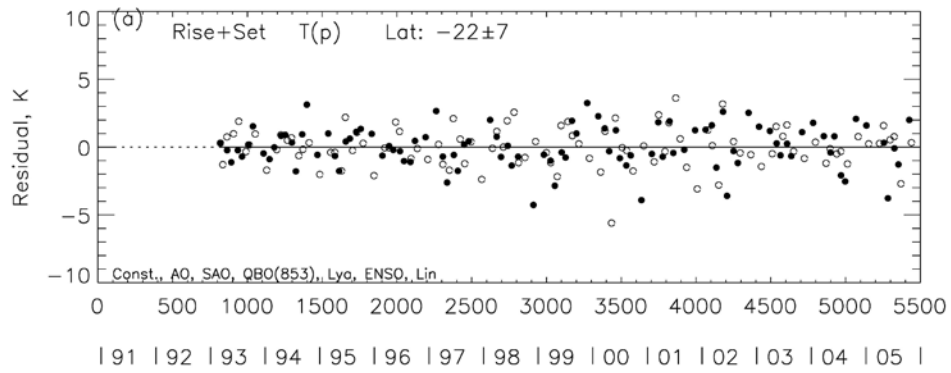


675

676 Figure 4—As in Figure 2, but for time series of HALOE $T(p)$ at 22.5°S at 0.5 hPa (top) and 2

677 hPa (bottom).

678



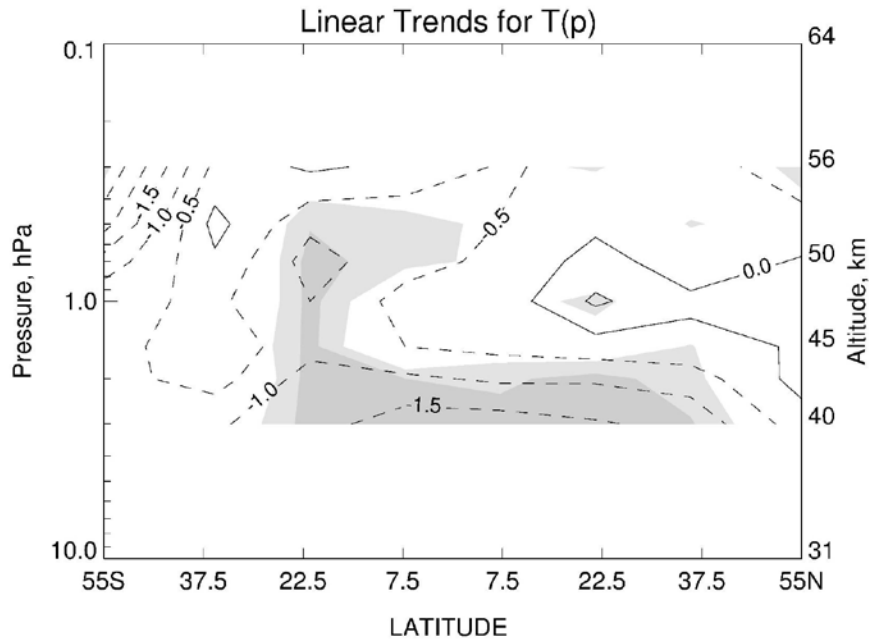
679

680 Figure 5—Time series of temperature residuals from the MLR model fit in Figure 4 at 2 hPa.

681

682

683



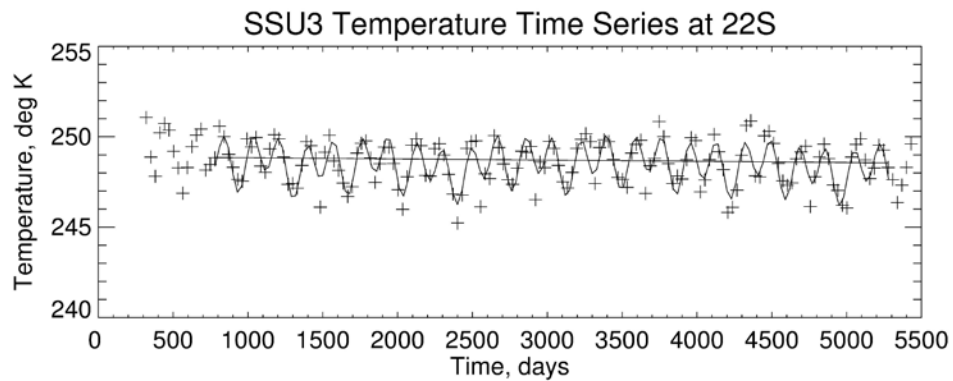
684

685 Figure 6—Distribution of HALOE temperature trends (K/decade). Dashed contours are
686 negative; contour interval is 0.5 K/decade. Dark shading denotes regions with confidence
687 intervals (CI)>90% and lighter shading is for 90%>CI>70%.

688

689

690



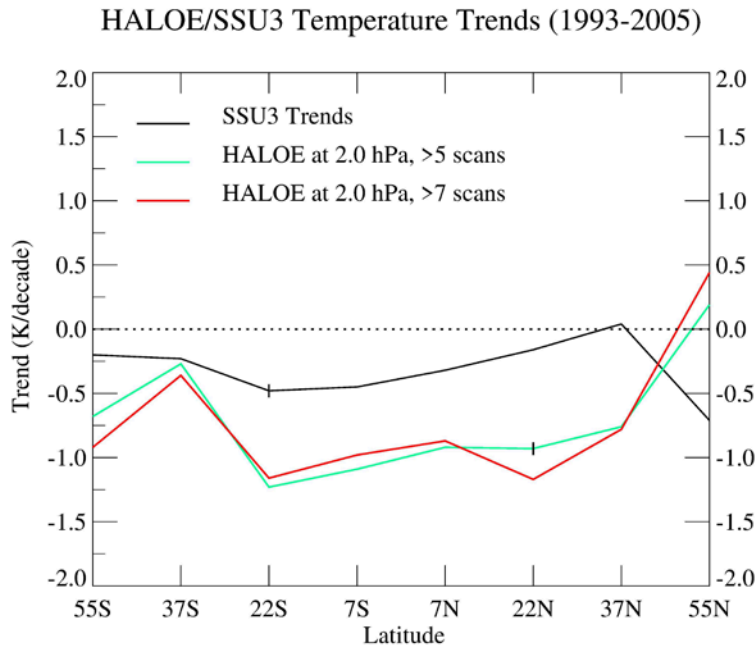
691

692 Figure 7—Temperature time series from merged SSU3 data and for a 15-degree wide latitude bin
693 centered at 22°S. The oscillating curve is the MLR fit to the data (+) and the terms of the model
694 are identical to those used for the analyses of the HALOE temperatures.

695

696

697



698

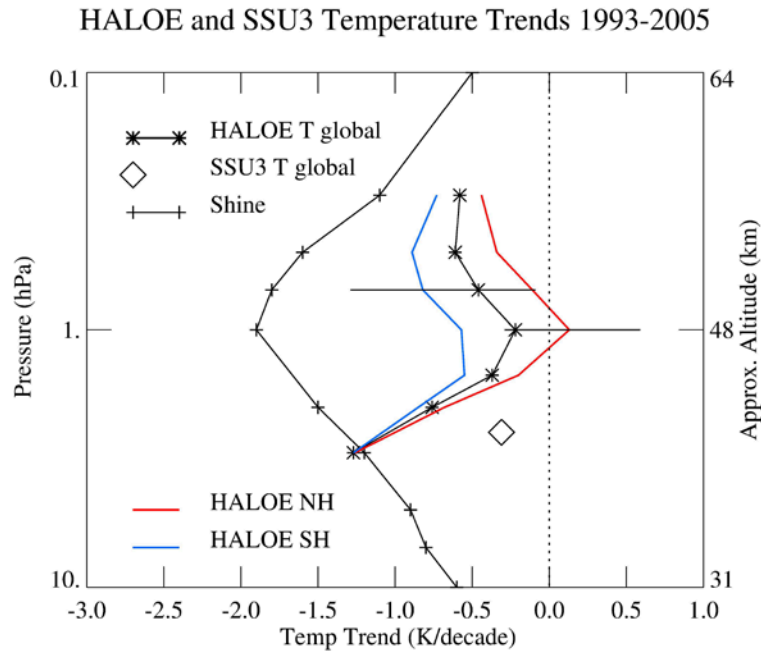
699 Figure 8—HALOE temperature trends versus latitude at 2.0 hPa in terms of K/decade. The
700 green and red curves show results from when more than 5 profiles or more than 7 profiles are
701 used to estimate the zonal or bin-averaged points. The solid curve shows the trends from the
702 merged SSU3 data of 1993-2005. Vertical bars at 22S and 22N are 2σ uncertainties from the
703 MLR trend analyses.

704

705

706

707



708

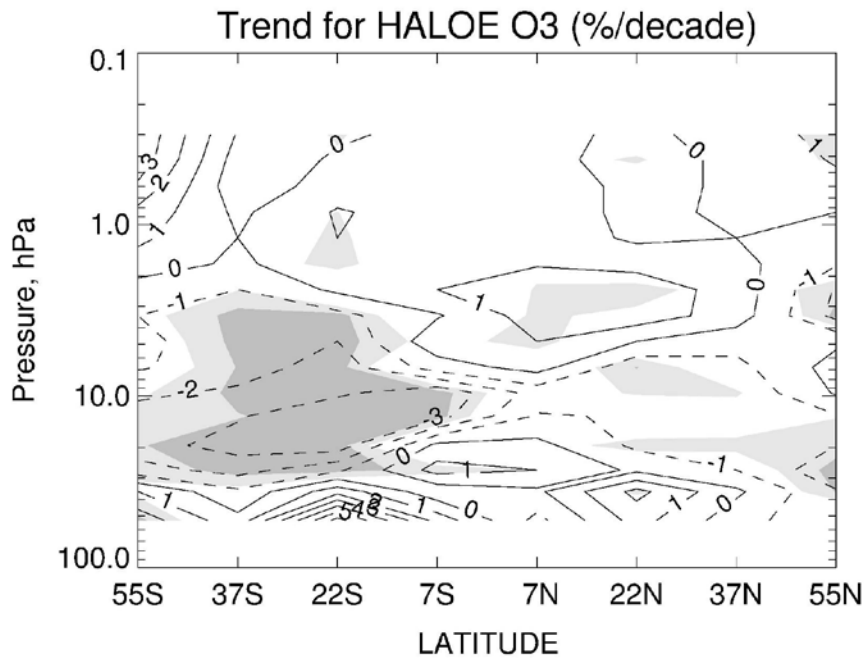
709 Figure 9—The near-global and separate hemispheric temperature profiles for the upper
710 stratosphere/lower mesosphere from HALOE, as compared with the total calculated T(p) trends
711 of Figure 1. Horizontal bars at 0.7 and 1.0 hPa denote the range of the trends within each
712 hemisphere. The pressure location of the SSU3 trend has an estimate of 2.5 hPa (see text).

713

714

715

716

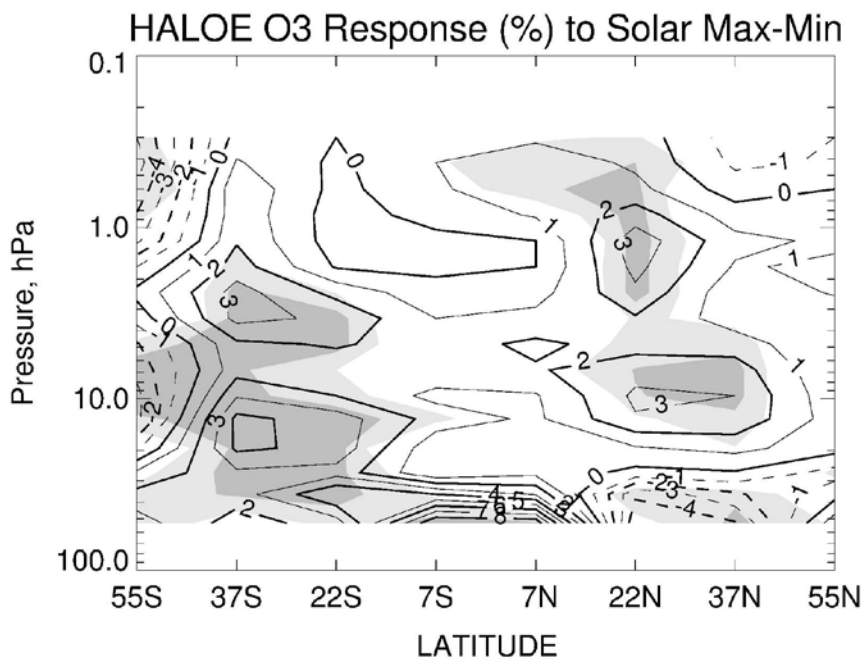


717

718 Figure 10—Trends of HALOE ozone mixing ratio in (%/decade). Dashed contours represent
719 negative trends; contour interval is 1%. Dark shading denotes regions with confidence intervals
720 (CI) > 90% and lighter shading is for 90% > CI > 70%.

721

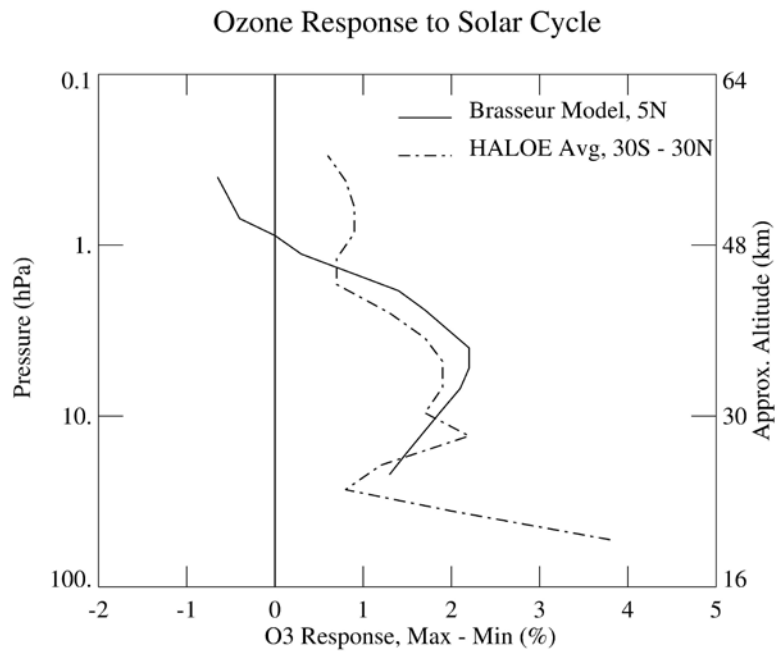
722



723

724 Figure 11—HALOE ozone response (in %) to max minus min solar forcings from a Lyman-
725 alpha proxy. Negative response contours are dashed; contour intervals are 1%. Shading
726 represents CI values as in Figure 10.

727

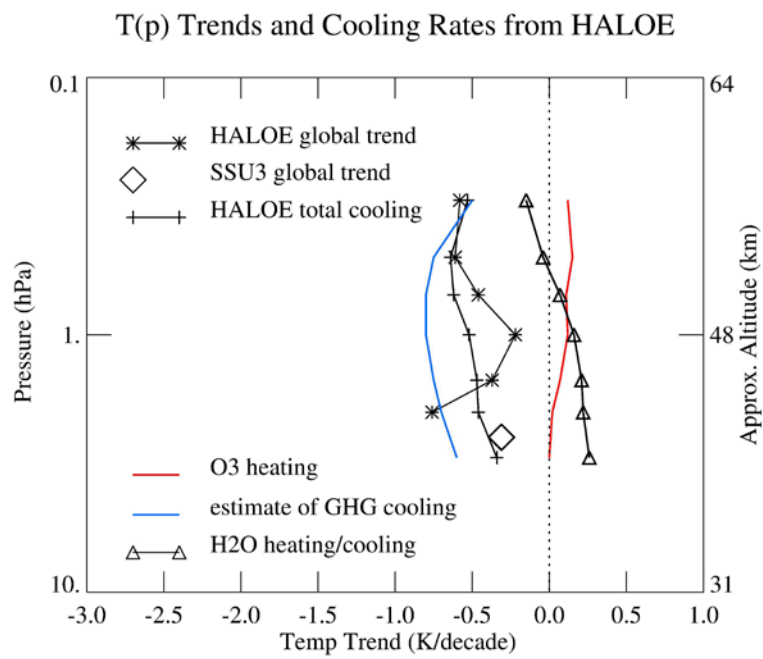


729

730 Figure 12—HALOE ozone response profile for the low latitudes and from the model of Brasseur
731 (1993).

732

733



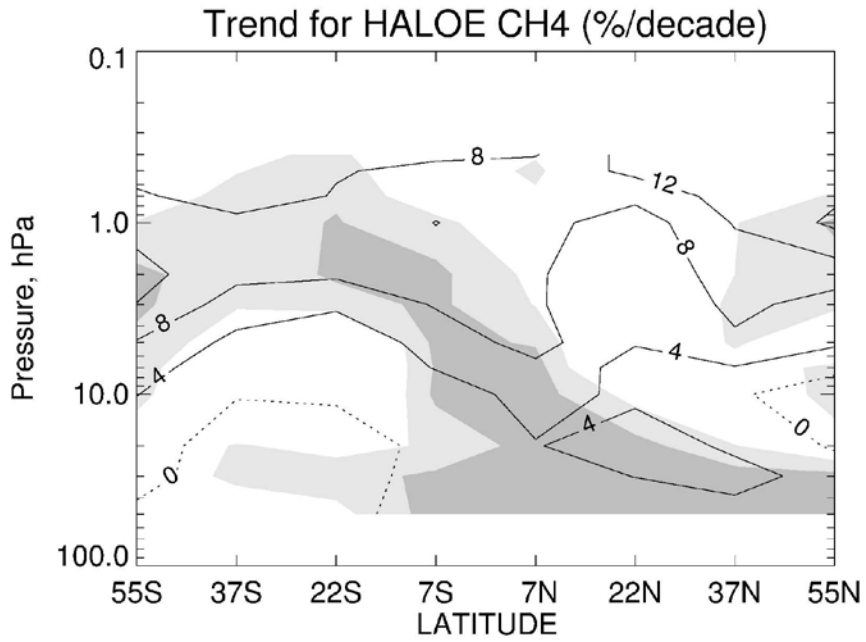
734

735 Figure 13—Comparison of the estimated total cooling profile with the near-global temperature
736 trend profiles from HALOE and from SSU3. There are separate contributions included from
737 HALOE O₃ (red) and H₂O and from the GHG (blue) in the estimated total cooling profile.

738

739

740



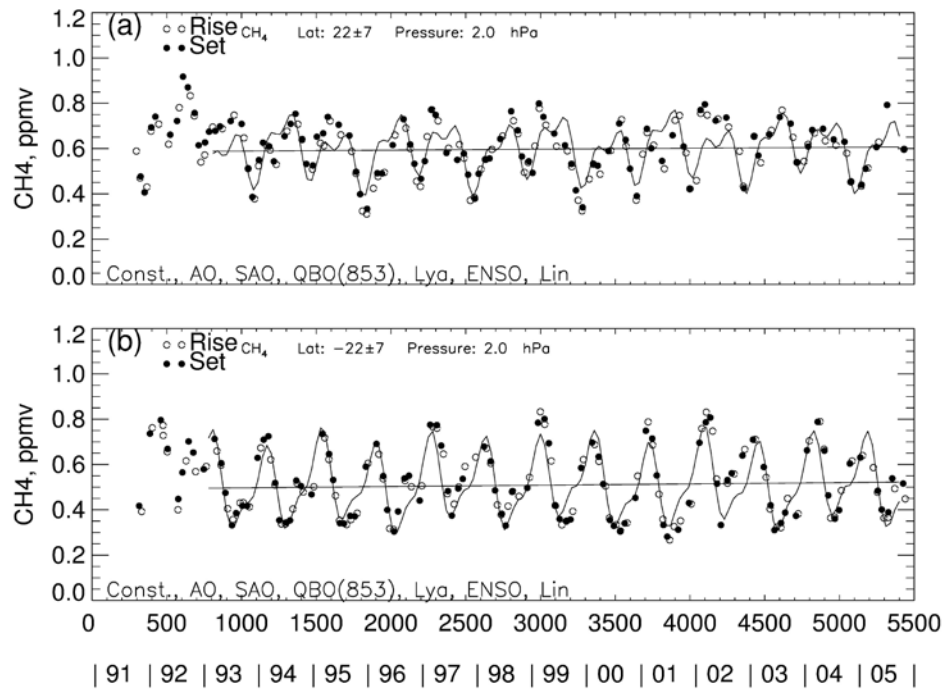
741

742 Figure 14—Distribution of trends (in %/decade) for HALOE CH₄ for 1993-2005. Contour
743 interval is 4 %/decade. Shading represents CI values as in Figure 10.

744

745

746



747

748 Figure 15—Time series at 2.0 hPa for HALOE methane at (top) 22.5°N and at (bottom) 22.5°S.

749